17th AIAA/CEAS Aeroacoustics Conference, 6–8 June 2011, Portland, Oregon, USA

Surface modes in sheared flow using the modified Myers boundary condition

Edward J. Brambley*
DAMTP, University of Cambridge, UK

This paper considers surface modes within a lined cylindrical duct with uniform flow apart from a thin boundary layer, using a modified Myers boundary condition. For a fixed frequency ω, this is shown to lead to up to six surface modes, rather than the maximum of four previously predicted for uniform flow. Solving for the frequency ω at a fixed wavelength (important for stability analysis), using a mass–spring–damper impedance model, gives up to eight surface modes using the Modified Myers Boundary Condition, rather than the maximum of six predicted for uniform flow. The different number of surface modes hints at new behaviour, particularly with respect to stability, and is also of use for frequency-domain mode-matching techniques, which depend on having found all relevant available modes during matching. Numerical examples are given comparing the predictions of the surface mode approximation to full solutions of the Pridmore-Brown equation.

I. Introduction

Consider, as a simplified mathematical model for the propagation of sound in an aeroengine intake or bypass, a cylindrical or annular acoustically-lined duct carrying a mean axial flow. The acoustic lining is represented by an impedance $Z = p/v$, where a pressure $p\exp\{\mathrm{i}\omega t\}$ produces a normal fluid velocity $v\exp\{\mathrm{i}\omega t\}$ through the lining. The simplest mean axial flow is a uniform flow, which would at first seem to be a good approximation for aeroengines owing to the high Reynolds numbers at which they operate. This situation has been extensively studied using the Myers,[1] or Ingard–Myers,[2] boundary condition, which incorporates both the impedance of the lining and the effect of slipping mean flow. This boundary condition has been shown by Eversman & Beckemeyer[3] and Tester[4] to correspond to the limit of a vanishingly-thin non-slip boundary layer over the lining.

There are two important features of this uniform flow over an impedance lining using the Myers boundary condition. The first is that, in addition to the acoustic modes (expected to be only slightly perturbed from their hard-walled counterparts), this system supports modes of a different nature localized close to the acoustic lining. These modes were aptly named *surface modes* and where investigated initially by Rienstra[5,6] and subsequently by Brambley & Peake.[7] For a locally-reacting boundary, meaning that Z is a function only of the frequency ω and is independent of wavelength, at any frequency there are up to four surface modes, one of which was tentatively suggested by Rienstra[6] as being a hydrodynamic instability. The second important feature of this uniform flow over an impedance lining using the Myers boundary condition is that it yields an illposed problem,[8] meaning that numerical simulations become unstable at the grid scale, that a stability analysis is not possible, and that frequency-domain simulations are of undetermined accuracy.

Recently, progress has been made on correcting this illposedness by incorporating a thin-but-nonzero thickness boundary layer over the lining, leading to so called *modified Myers boundary conditions* by Rienstra & Darau,[9,10] Joubert,[11] and Brambley.[12,13] These boundary conditions remove the illposedness while still retaining the simplicity of a uniform flow, with the thin-but-nonzero-thickness boundary layer being incorporated within the boundary condition. (It should be noted that the modified Myers boundary conditions are restricted to having thin boundary layers, and also ignore the effect of the critical layer within the

*Research Fellow, Department of Applied Mathematics & Theoretical Physics, University of Cambridge, CMS, Wilberforce Road, Cambridge CB3 0WA, United Kingdom. AIAA member.

boundary layer; see Brambley, Darau & Rienstra[14] for further details.) The effective modified impedance Z_{mod} that modified Myers boundary conditions lead to is in general a function of both frequency ω and axial wavenumber k (and, indeed, azimuthal wavenumber m), even when the underlying impedance of the liner is locally-reacting and therefore depends only on ω. This dependence causes an increased number of surface modes above the four previously predicted; this has been shown for a thin cylindrical shell whos impedance includes a k^4 term, leading to up to ten surface modes for any given frequency.[15]

The number and behaviour of the surface modes is of the utmost importance for verifying that a mode-matching scheme is considering all appropriate modes, and for stability analysis. For stability analyses this is particularly pertinent, since an absolute instability is given using the Briggs–Bers criterion[16,17] by the collision of two modes in the k-plane as $\mathrm{Im}(\omega)$ is varied, and hence if there are more surface modes there is more potential for an absolute instability to be present.

II. Mathematical derivation

What follows is applicable to a cylindrical, annular, or planar lined surface, although for definiteness here we will consider the cylindrical case only. The cylinder axis is in the x-direction with the cross-section defined by polar coordinates r, θ. Nondimensionalizing by the duct radius, the centreline mean-flow sound speed and the centreline mean-flow density gives the mean-flow centreline velocity as the Mach number M. On top of this mean flow we consider a potential perturbation

$$\boldsymbol{u} = M\boldsymbol{e_x} + \boldsymbol{\nabla}\phi, \qquad \rho = 1 - \frac{\mathrm{D}\phi}{\mathrm{D}t}, \qquad p = p_0 - \frac{\mathrm{D}\phi}{\mathrm{D}t}, \tag{1}$$

where $\mathrm{D}/\mathrm{D}t = \partial/\partial t + M\partial/\partial x$ is the convective derivative with respect to the mean flow and p_0 is the constant mean flow pressure. The potential ϕ is given by

$$\phi = p_m(r;\omega,k)\exp\{\mathrm{i}\omega t - \mathrm{i}kx - \mathrm{i}m\theta\}, \tag{2}$$

where, for a cylindrical duct,

$$p_m(r;\omega,k) = \mathrm{J}_m(\alpha r) \qquad \alpha^2 = (\omega - Mk)^2 - k^2, \tag{3}$$

where J_m is the m^{th} Bessel function of the first kind. The Myers boundary condition becomes

$$1 - \frac{(\omega - Mk)^2}{\mathrm{i}\omega Z_{\mathrm{mod}}}\frac{J_m(\alpha)}{\alpha J_m'(\alpha)} = 0, \tag{4}$$

with $Z_{\mathrm{mod}} = Z$, giving allowable values for α and therefore the allowable axial wavenumbers k. Here, we will use the modified Myers boundary condition of Brambley (Eq. 7 of Ref. 12 or Eq. 9 of Ref. 13), modelling a thin non-slip boundary layer of thickness $O(\delta)$ at the lining. This also leads to the boundary condition (4), but with

$$\mathrm{i}\omega Z_{\mathrm{mod}} = \mathrm{i}\omega Z\left[1 - \big(k^2+m^2\big)\delta I_1\frac{\mathrm{J}_m(\alpha)}{\alpha \mathrm{J}_m'(\alpha)}\right] + \omega^2\delta_{\mathrm{mass}} - 2\omega kM\delta_{\mathrm{mom}} + k^2M^2\delta_{ke} + O\big(\delta^2\big), \tag{5}$$

or, equivalently,

$$\mathrm{i}\omega Z_{\mathrm{mod}} = \mathrm{i}\omega Z - (\mathrm{i}\omega Z)^2\delta I_1\frac{k^2+m^2}{(\omega-Mk)^2} + \omega^2\delta_{\mathrm{mass}} - 2\omega kM\delta_{\mathrm{mom}} + k^2M^2\delta_{ke} + O\big(\delta^2\big), \tag{6}$$

where

$$\delta_{\mathrm{mass}} = \int_0^1 1 - R(r)\,\mathrm{d}r, \qquad \delta_{\mathrm{mom}} = \int_0^1 1 - \frac{R(r)U(r)}{M}\,\mathrm{d}r, \qquad \delta_{\mathrm{ke}} = \int_0^1 1 - \frac{R(r)U(r)^2}{M^2}\,\mathrm{d}r, \tag{7}$$

$$\delta I_1 = \int_0^1 1 - \frac{(\omega-Mk)^2}{\big(\omega - U(r)k\big)^2R(r)}\,\mathrm{d}r \quad \sim \quad \frac{\delta_1 Mk}{\omega} \quad \text{for} \quad k/\omega \gg 1, \tag{8}$$

$U(r)$ and $R(r)$ are the velocity and density of the mean-flow including the boundary layer, and $\delta_1 = -M/\big(R(1)U'(1)\big)$. Note that all δ quantities are of the order of the boundary layer thickness and so are

small, and that $\delta_{\rm mass}$, $\delta_{\rm mom}$ and $\delta_{\rm ke}$ are the mass, momentum and kinetic energy thicknesses of the boundary layer respectively, while δ_1 is also some sort of measure of boundary layer thickness. Here, we will use the asymptotic result of Ref. 13 for δI_1 given in (8), while noting that this approximation of δI_1 is in the relevant regime for surface modes and is exact for a linear boundary layer profile (such as assumed by Rienstra & Darau[10] for their modified Myers boundary condition).

The surface mode dispersion relation we use here is from Ref. 7, which is an extension of that given by Rienstra[6] to correct for nonzero m. In slightly different notation to Ref. 7, the surface mode dispersion relation is

$$\mu - \frac{(\omega - Mk)^2}{\mathrm{i}\omega Z_{\rm mod}} = 0 \qquad \text{where} \quad \mu^2 = k^2 + m^2 - (\omega - Mk)^2, \tag{9}$$

and $\mathrm{Re}(\mu)$ is required positive, since the eigenfunction for this surface mode is asymptotically $p_m(r;\omega,k)/p_m(1;\omega,k) \sim \exp\{-(1-r)\mu\}$ and is required to decay away from the surface. Since $\mathrm{J}_m(\alpha)/\big(\alpha \mathrm{J}'_m(\alpha)\big) = p_m(1)/p'_m(1) \sim 1/\mu$, Eq. (9) for the modified Myers boundary condition becomes

$$\mu - \frac{(\omega - Mk)^2}{\mathrm{i}\omega Z\Big(1 - \delta_1\big(k^2+m^2\big)Mk/(\omega\mu)\Big) + \omega^2\delta_{\rm mass} - 2\omega k M \delta_{\rm mom} + k^2 M^2 \delta_{ke}} = 0. \tag{10}$$

This may be rearranged to give

$$\begin{aligned}\big(\mathrm{i}\omega Z + \omega^2\delta_{\rm mass} - 2\omega k M\delta_{\rm mom} + k^2M^2\delta_{ke}\big)^2\big(k^2+m^2-(\omega-Mk)^2\big)\omega^2 \\ - \big(\mathrm{i}\omega Z\delta_1\big(k^2+m^2\big)Mk + \omega(\omega-Mk)^2\big)^2 = 0.\end{aligned} \tag{11}$$

Assuming that Z is locally reacting, so that Z is independent of k and m, then (11) gives a polynomial in k of degree six, so that there are six surface modes, although due to the restriction that $\mathrm{Re}(\mu) > 0$ not all of these may be physical for all values of Z; a similar argument was used in Refs. 6 and 7. Indeed, the results of these two papers are recovered by setting the δ-quantities in (11) to zero, yielding a polynomial of degree four and therefore leading to four surface modes. If Z is given by a mass–spring–damper model, so that $\mathrm{i}\omega Z$ is a polynomial of degree two in ω, then for fixed k Eq. (11) gives a polynomial in ω of degree eight, so that there are eight possible surface modes in ω for fixed k. This compares to the unmodified Myers result of six surface modes, obtained by setting the δ-quantities in (11) to zero.

The limitations of (10) should be borne in mind: that δI_1 is evaluated using the asymptotics given in (8) which are only valid for $k/\omega \gg 1$; that the surface mode dispersion relation (9) is only valid for $\mathrm{Re}(\mu) \gtrsim O(1)$; that, since the surface modes have $J_m(\alpha r)/\mathrm{J}_m(\alpha) \sim \exp\{-(1-r)\mu\}$, the modified Myers boundary condition (5) is only valid for surface modes provided $|\mu| \lesssim O(1/\delta)$, where δ is a typical boundary layer thickness; and that the modified Myers boundary condition (5) ignores the critical layer within the boundary layer. These last two limitations are the most serious, and to avoid them requires a different analysis, such as given in Ref. 14 for a constant-then-linear boundary layer profile of constant density.

A. Rescaling the surface mode dispersion relation

We may simplify the dispersion relation (11), reducing the number of free parameters by one, by introducing renormalized variables,

$$\begin{aligned}&\tilde\mu = \mu/m, && \beta = +\sqrt{1-M^2}, && \sigma = M + \beta^2 k/\omega, && \lambda = \omega/(m\beta),\\ &\tilde h = 2\omega\delta_{\rm mom}, && \Delta_{\rm mass} = \delta_{\rm mass}/(2\delta_{\rm mom}), && \Delta_{\rm ke} = \delta_{\rm ke}/(2\delta_{\rm mom}), && \Delta_1 = \delta_1/(2\delta_{\rm mom}).\end{aligned} \tag{12}$$

The *reduced axial wavenumber* σ was introduced by Rienstra[6] to remove the mean flow dependence from the axial wavenumber k, while $(\tilde\mu, \beta, \sigma, \lambda)$ are the same as $(\mu, \beta, \sigma, \lambda)$ in Ref. 7. Using these, and assuming $m > 0$, gives

$$\tilde\mu^2 = 1 - \lambda^2\big(1-\sigma^2\big) \qquad \text{with} \quad \mathrm{Re}(\tilde\mu) > 0, \tag{13}$$

while (10) gives the rescaled dispersion relation

$$\frac{\tilde\mu}{\beta\lambda} - \frac{(1-M\sigma)^2 + \mathrm{i}Z\tilde h\Delta_1 M(\sigma-M)\Big((\sigma-M)^2/\beta^2 + 1/\lambda^2\Big)}{\mathrm{i}Z\beta^4 + \tilde h\big[\Delta_{\rm mass}\beta^4 - M\beta^2(\sigma-M) + M^2\Delta_{\rm ke}(\sigma-M)^2\big]} = 0. \tag{14}$$

Line	Change in number of surface modes			
	$\mathcal{R}_1$	$\mathcal{R}_2$	$\mathcal{R}_3$	$\mathcal{R}_4$
ℓ_1			-1	
ℓ_2		+1		
ℓ_3		+1		
ℓ_4				+1
ℓ_5		-1		
ℓ_6			+1	
ℓ_7	+1			

Table 1. The number and position of actual surface modes for varying Z shown in figure 1. If a line labelled ℓ_i is crossed in the direction of the arrow shown in figure 1, then the number of actual surface modes in the regions $\mathcal{R}_i$ shown in figure 1*c* change by the amount shown in this table.

The free parameters governing the behaviour of the surface modes are therefore the liner impedance Z, the acoustic parameter λ, the flow parameters M and $\tilde{h}$, and the boundary layer shape parameters Δ_{mass}, Δ_{ke}, and Δ_1. A constant-then-linear boundary layer profile with constant density,

$$U(r) = \begin{cases} M & r < 1-h \\ M(1-r)/h & r > 1-h \end{cases} \qquad R(r) \equiv 1, \tag{15}$$

gives $\Delta_{\text{mass}} = 0$, $\Delta_{\text{ke}} = 2/3$ and $\Delta_1 = 1$, with $\tilde{h} = \omega h$.

III. Solutions of the surface mode dispersion relation

In this section, we investigate the number and position of surface modes for a given frequency ω, and how these vary with varying impedance Z. The procedure we follow is similar to that described by Rienstra[6] and was also used in Ref. 7.

For a locally-reacting impedance, meaning that Z is independent of k and m, the surface mode dispersion relation (11) (or equivalently (14)) is of sixth order in k (or σ), and therefore there are six potential surface modes for a given frequency ω. However, not all of these potential surface modes will satisfy the requirement that $\text{Re}(\mu) > 0$. The number of actual surface modes will therefore change when one of the potential surface modes moves from having $\text{Re}(\mu) < 0$ to $\text{Re}(\mu) > 0$. We may therefore map the curve $\text{Re}(\mu) = 0$ into the complex Z-plane to denote regions of the Z-plane that have the same number of actual surface modes. Moreover, since only impedances that satisfy $\text{Re}(Z) > 0$ remove energy from the fluid and are hence physical, we may map the curve $\text{Re}(Z) = 0$ into the complex σ plane to separate regions of the σ plane that can and cannot contain surface modes.

Figure 1 plots $\text{Re}(\mu) = 0$ and $\text{Re}(Z) = 0$ in the complex Z and σ planes. The parameters used were chosen to correspond to rotor-alone tones in a typical aeroengine at takeoff, with $M = 0.5$, $\omega = 31$ and $m = 24$, with a boundary layer of thickness $\delta = 10^{-3}$ and a tanh profile, as used by Rienstra & Vilenski,[18]

$$U(r)/M = \tanh\left(\frac{1-r}{\delta}\right) + \big(1 - \tanh(1/\delta)\big)\left(\frac{1+\tanh(1/\delta)}{\delta} r + (1+r)\right)(1-r), \tag{16}$$

with constant density $R(r) \equiv 1$. The boundary layer parameters for this situation are

$$\begin{array}{cccc} \delta_{\text{mom}} = 6.9315 \times 10^{-4} & \delta_{\text{ke}} = 10^{-3} & \delta_1 = 10^{-3} & \delta_{\text{mass}} = 0 \\ \tilde{h} \approx 4.3 \times 10^{-2} & \Delta_{\text{ke}} \approx 0.72135 & \Delta_1 \approx 0.72135 & \Delta_{\text{mass}} = 0 \end{array}$$

The situation is rather complicated, and is described in table 1. For large $|Z|$ there are two actual surface modes present, located in regions $\mathcal{R}_1$ and $\mathcal{R}_3$ of the σ-plane, as shown in figure 1*c*. As Z varies and crosses the lines labelled ℓ_i in figure 1*a,b*, other actual surface modes appear. In total, there are a maximum of two surface modes possible in each of regions $\mathcal{R}_1$ and $\mathcal{R}_2$, and a maximum of one surface mode possible in each of regions $\mathcal{R}_3$ and $\mathcal{R}_4$. In each of regions $\mathcal{R}_1$ and $\mathcal{R}_2$, the two actual surface modes can be made to collide

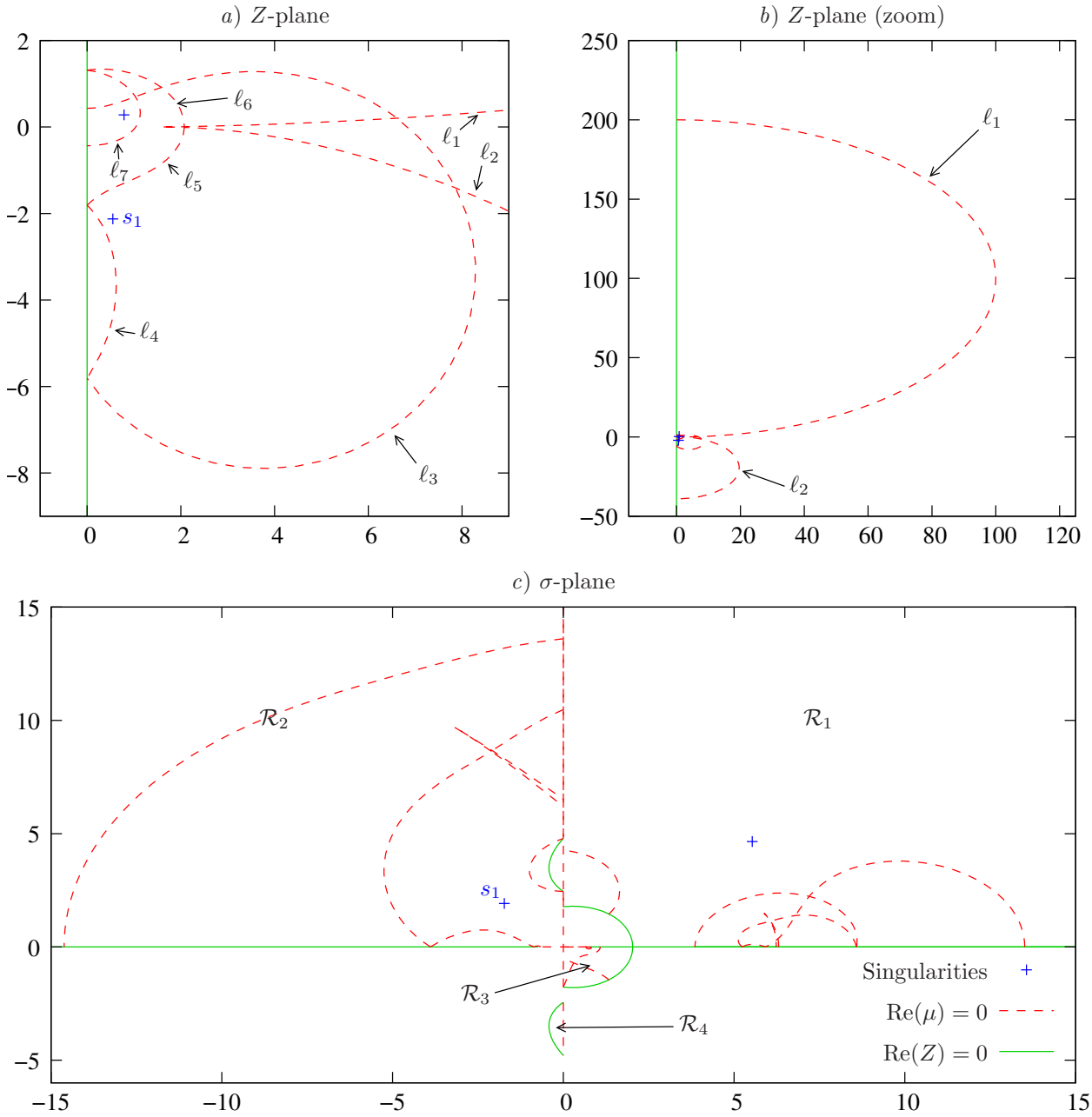

Figure 1. Plots of $\mathrm{Re}(\mu) = 0$ and $\mathrm{Re}(Z) = 0$ in the Z- and σ-planes using the surface mode dispersion relation (11), for a tanh boundary layer profile given by (16) with $\delta = 10^{-3}$ and $M = 0.5$, for $\omega = 31$ and $m = 24$ (giving $\lambda \approx 1.49$). Singularities are where the dispersion relation admits a double root. Lines labelled ℓ_i, regions labelled $\mathcal{R}_j$, and the singularity labelled s_1 are described in the text.

by picking a particular value of Z, labelled as singularities in figure 1*a*, with the locations in the σ-plane that these collisions occur plotted in figure 1*c*. It is hypothesised here that the singularity in the $\mathcal{R}_1$ plane may be linked to a possible absolute instability, although this is not investigated further.

Since figures 1*a,c* do not look like their equivalent with uniform flow (see, e.g., figure 2 of Ref. 7), it is interesting to note how the uniform flow equivalents are recovered in the limit $\tilde{h} \to 0$ by making the boundary layer progressively thinner. Figure 2 shows the comparable diagrams to figures 1*a,c* for the same parameters but for a tanh boundary layer with thicknesses $\delta = 3 \times 10^{-4}$, and $\delta = 2.5 \times 10^{-4}$ and $\delta = 5 \times 10^{-5}$, by which time the $\lambda = 1.5$ solution from figure 2 of Ref. 7 is becoming recognizeable.

This section has described the position and number of surface modes for the particular values $\lambda \approx 1.5$, $M = 0.5$, $\tilde{h} \approx 0.043$, and a tanh boundary layer profile. Due to space and time constraints, no further analysis of different parameter regimes has been attempted; however, it is expected that the situation described here is indicative of a relatively large and aeroacoustically-useful range of parameters. In the next section, we compare the predictions of this surface mode thin-boundary-layer approximation to full numerical solutions of the Pridmore-Brown equation.

IV. Numerical comparison

In this section, we consider the frequency ω to be given and solve for the axial wavenumber k. We will compare the predictions of the modified Myers surface mode (MMSM) dispersion relation (11), as discussed in the previous section, with a number of progressively less approximate dispersion relations. The first of these we term the *Short Wavelength Modified Myers* (SWMM) dispersion relation, being the dispersion relation (4) with Z_{mod} given by (5) and with the short wavelength approximation $\delta I_1 \sim \delta_1 Mk/\omega$. Similarly, the *Full Modified Myers* (FMM) dispersion relation is given by (4) with Z_{mod} given by (5) but with the δI_1 integral being computed numerically.

As a check on the accuracy of these modified Myers boundary conditions, we will also consider the dispersion relation given by solving the Pridmore-Brown[19] equation numerically. The Pridmore-Brown equation is a direct rearrangement of the Linearized Euler Equations in the frequency domain, eliminating all but the linearized pressure $\tilde{p}$, giving

$$\tilde{p}'' + \left(\frac{1}{r} + \frac{2kU'}{\omega - Uk} - \frac{R'}{R} \right) \tilde{p}' + \left((\omega - Uk)^2 R - k^2 - \frac{m^2}{r^2} \right) \tilde{p} = 0, \tag{17}$$

where a prime denotes $\mathrm{d}/\mathrm{d}r$. The boundary conditions are regularity of $\tilde{p}$ at $r = 0$ and the impedance boundary condition (assuming $U(1) = 0$),

$$Z\tilde{p}'(1) + \mathrm{i}\omega R(1)\tilde{p}(1) = 0.$$

The Pridmore-Brown dispersion relation (labelled *PB* in the figures) is given by finding a value of k such that (17) subject to these boundary conditions possesses a nonzero solution. Eq. (17) was solved using a 12th order implicit central finite difference method, with grid points clustered so as to provide sufficient resolution within even very thin boundary layers (the same code was used for the numerical results in Ref. 13); typically 4000 radial points were used. The boundary condition at $r = 1$ was then satisfied using a Newton-Raphson iteration to find the modal wavenumber k, with iteration starting points chosen close to predicted positions of modes and on an evenly spaced grid to find unpredicted modes.

Since the asymptotics of Ref. 13, leading to the modified Myers boundary condition given in (4) and (5), are based on the Pridmore-Brown equation to first order in the boundary layer thickness, what follows also provides a useful comparison of the accuracy of this boundary condition. For comparison, we also include here the results of the unmodified Myers boundary condition (labelled *Myers* in the figures), given by the dispersion relation (4) with $Z_{\mathrm{mod}} = Z$, and the unmodified surface mode dispersion relation which follows from it[6,7] (labelled as *UMSM* in the figures).

We consider here two different parameters, namely $(\omega, m) = (31, 24)$ and $(\omega, m) = (10, 5)$. For all cases here, the boundary layer thickness is 10^{-3} and the centerline Mach number is $M = 0.5$. Two boundary layer profiles are used: the *linear* profile given by (15), with the thickness defined to be h, and the *tanh* profile given by (16), with the thickness defined to be δ; note that this gives $\delta_1 = 10^{-3}$ in both cases.

Figure 3 shows the allowable axial wavenumbers for $(\omega, m) = (10, 5)$ with a tanh boundary layer profile and an impedance wall with $Z = 1 - 2.5\mathrm{i}$. In this case, the surface mode dispersion relation (11) correctly

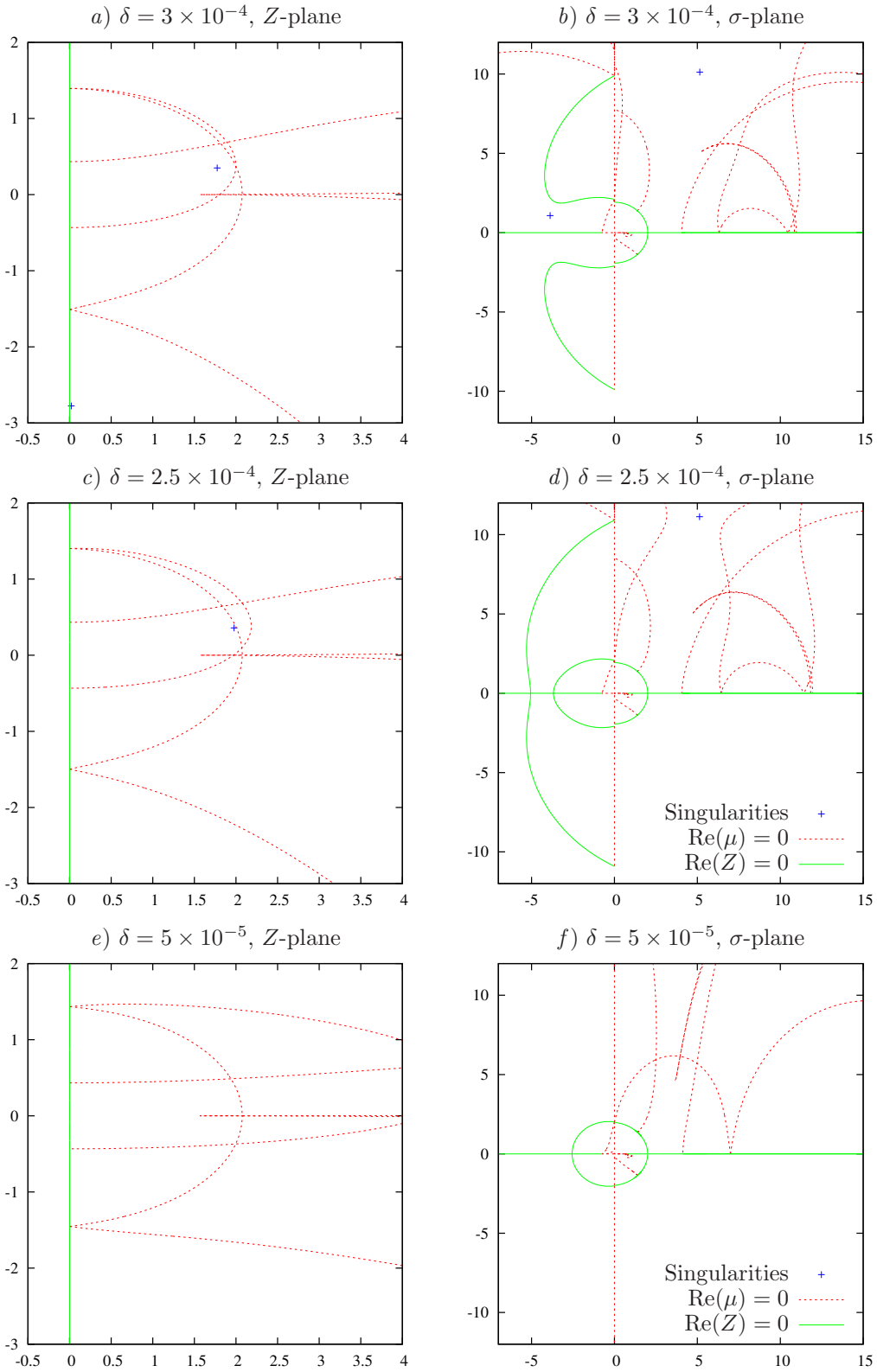

Figure 2. The curves $\mathrm{Re}(Z) = 0$ and $\mathrm{Re}(\mu) = 0$ plotted in the complex Z- and σ-planes, for the same parameters as figure 1 but with different boundary layer thicknesses. The boundary layer has a tanh profile given by (16) with thickness δ and $M = 0.5$, for $\omega = 31$ and $m = 24$ (giving $\lambda \approx 1.49$).

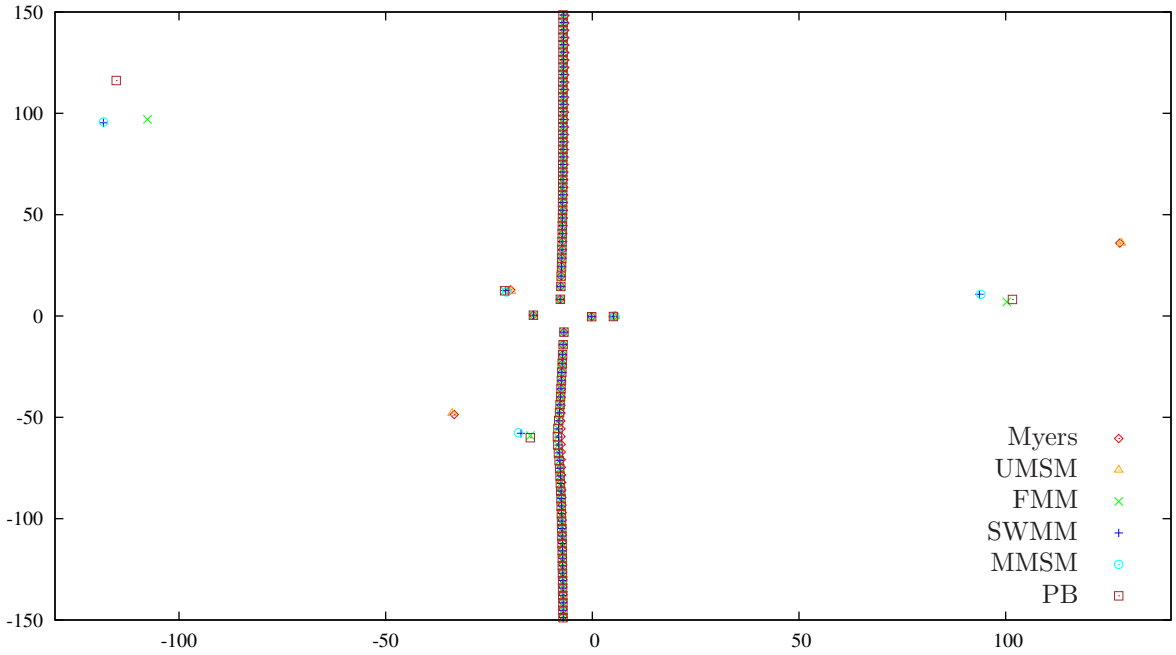

Figure 3. Axial wavenumbers (k) in the complex k-plane for a boundary impedance $Z = 1 - 2.5\mathrm{i}$ and various dispersion relations, for $\omega = 10$, $m = 5$, and a tanh boundary layer profile (16) with $\delta = 10^{-3}$. Dispersion relations: UMSM = Unmodified Myers Surface Mode, FMM = Full Modified Myers, SWMM = Short Wavelength Modified Myers, MMSM = Modified Myers Surface Mode, PB = Pridmore-Brown numerical modes.

predicts the existence and location of five actual surface modes: two in region $\mathcal{R}_2$ (the top-left quadrant of the k-plane) and one in each of regions $\mathcal{R}_1$, $\mathcal{R}_3$ and $\mathcal{R}_4$. The unmodified Myers boundary condition predicts only four actual surface modes, of which the locations of only two are predicted accurately.

Figure $4a$ uses similar parameters to figure 3 but for the impedance $Z = 1.6+0.2\mathrm{i}$. In this case, the surface mode dispersion relation (11) correctly predicts the existence of two surface modes in region $\mathcal{R}_1$. This is significant, as the surface mode analysis for uniform flow using the Myers boundary condition (Refs. 6 and 7) predicts only one in this quadrant, which Rienstra[6] tentatively predicted to be a hydrodynamic instability, and which appears to be confirmed by recent investigations.[10,13] Figure $4b$ shows the same situation but with a linear boundary layer profile, for which the short wavelength approximation for δI_1 becomes exact. While the surface modes (both numerically-calculated and predicted) move a moderate amount under this change, what is most striking is that there is one surface mode that is present for the tanh case (figure $4a$) and not present for the linear case (figure $4b$), despite all the approximations predicting it to be present in both cases. The track taken by this mode as the flow velocity $U(r)$ is linearly interpolated between the tanh and linear profiles is shown in both figures $4a$ and b, clearly demonstrating that this mode has disappeared and become an ordinary cut-off acoustic mode, and eliminating the possibility that the numerics has failed to find this mode for the linear profile.

We now consider the parameters $(\omega, m) = (31, 24)$, motivated by their relevance to rotor-alone noise in an aeroengine intake. Figure 5 is a similar plot to figure 4, but for $(\omega, m) = (31, 24)$ and $Z = 0.6-2\mathrm{i}$. The surface mode dispersion relation (11) correctly predicts two actual surface modes in region $\mathcal{R}_2$, one in $\mathcal{R}_3$ and none in $\mathcal{R}_4$, while the uniform flow dispersion relations incorrectly predict a surface mode in region $\mathcal{R}_4$ and fail to predict the second surface mode in region $\mathcal{R}_2$. However, the most interesting behaviour is seen in region $\mathcal{R}_1$ (the upper-right quadrant of the k-plane). The uniform flow dispersion relations predict a surface mode in this region, but inaccurately predict its location. The modified surface mode dispersion relation (11) predicts a surface mode much closer to the real k axis, which is backed up by the short wavelength approximation. However, this surface mode is only present for the full modified Myers dispersion relation and the numerical solution of the Pridmore-Brown equation for a linear boundary layer profile. Tracking this mode as the mean velocity $U(r)$ is linearly varied from a linear to tanh profile shows that this mode disappears into the critical layer branch cut located on the real k axis (see Ref. 14 for further details of the critical layer).

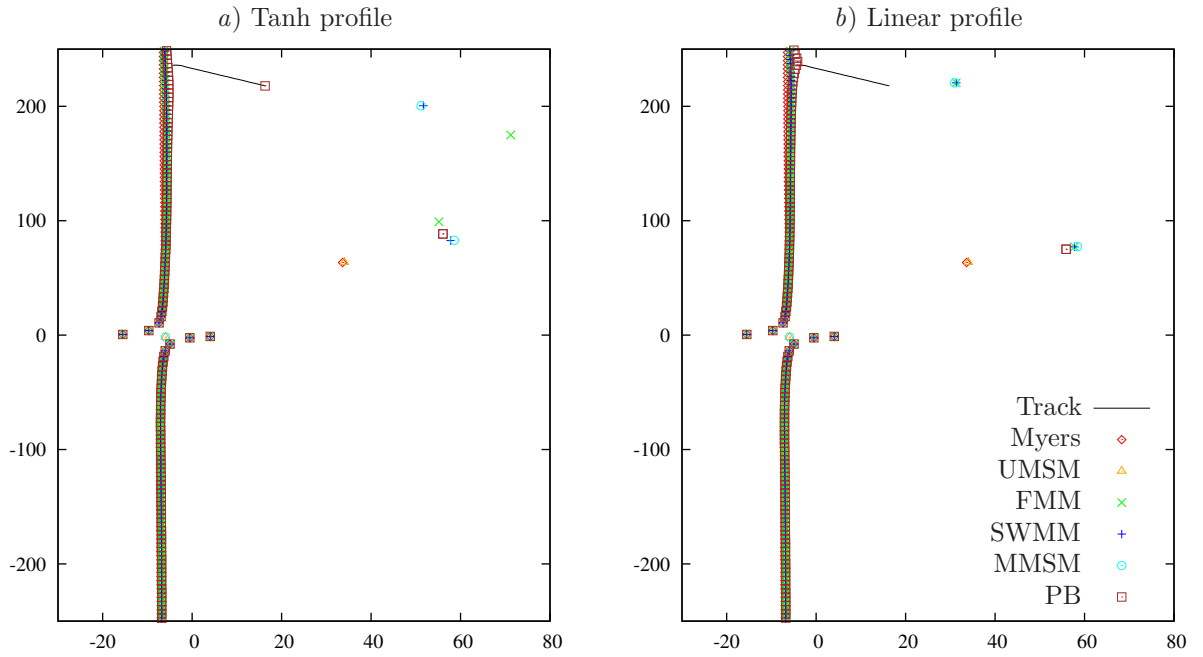

Figure 4. Axial wavenumbers (k) in the complex k-plane for a boundary impedance $Z = 1.6 + 0.2\mathrm{i}$ and various dispersion relations, for $\omega = 10$, $m = 5$, and *a*) a tanh boundary layer profile (16) with $\delta = 10^{-3}$, and *b*) a linear boundary layer profile (15) with $h = 10^{-3}$. "Track" refers to the motion of one particular PB numerical mode as the boundary layer profile is smoothly deformed from tanh to linear. Dispersion relations: UMSM = Unmodified Myers Surface Mode, FMM = Full Modified Myers, SWMM = Short Wavelength Modified Myers, MMSM = Modified Myers Surface Mode, PB = Pridmore-Brown numerical modes.

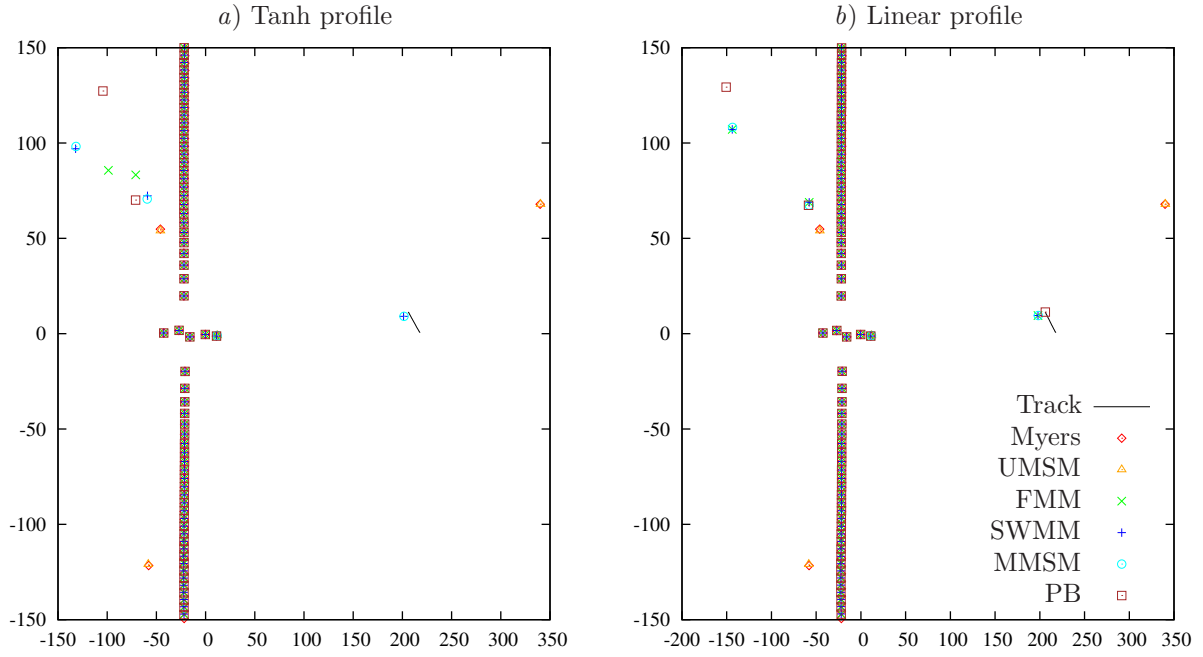

Figure 5. Axial wavenumbers (k) in the complex k-plane for a boundary impedance $Z = 0.6 - 2\mathrm{i}$ and various dispersion relations, for $\omega = 31$, $m = 24$, and *a*) a tanh boundary layer profile (16) with $\delta = 10^{-3}$, and *b*) a linear boundary layer profile (15) with $h = 10^{-3}$. "Track" refers to the motion of one particular PB numerical mode as the boundary layer profile is smoothly deformed from tanh to linear. Dispersion relations: UMSM = Unmodified Myers Surface Mode, FMM = Full Modified Myers, SWMM = Short Wavelength Modified Myers, MMSM = Modified Myers Surface Mode, PB = Pridmore-Brown numerical modes.

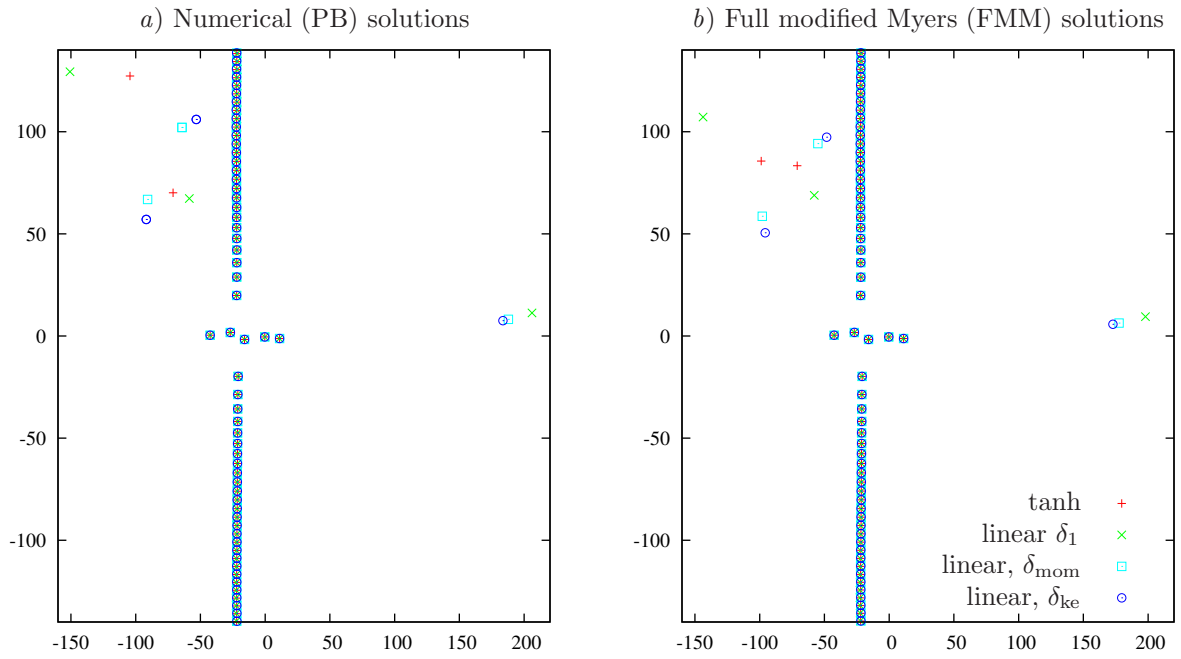

Figure 6. Axial wavenumbers (k) in the complex k-plane for four different boundary layers: a tanh profile with $\delta = 10^{-3}$, a linear profile with $h = 10^{-3}$ (matching the δ_1 of the tanh profile), a linear profile with $h = 1.39 \times 10^{-3}$ (matching the $\delta_{\rm mom}$ of the tanh profile), and a linear profile with $h = 1.5 \times 10^{-3}$ (matching the $\delta_{\rm ke}$ of the tanh profile). *a*) numerical solutions to the Pridmore-Brown equation (labelled PB in figure 5); *b*) full modified Myers solutions (labelled FMM in figure 5). Other parameters are as for figure 5: $M = 0.5$, $\omega = 31$, $m = 24$, and $Z = 0.6 - 2\mathrm{i}$.

Note that the tanh profile used in figures 4 and 5 has $\delta_{\rm mass} = 0$, $\delta_{\rm mom} \approx 7 \times 10^{-4}$, $\delta_{\rm ke} = 10^{-3}$ and $\delta_1 = 10^{-3}$, while the linear profile used in these figures has $\delta_{\rm mass} = 0$, $\delta_{\rm mom} = 5 \times 10^{-4}$, $\delta_{\rm ke} \approx 7 \times 10^{-4}$ and $\delta_1 = 10^{-3}$. It might be though, therefore, that the differences between the linear- and tanh-profile results in figures 4 and 5 might be due to the two boundary layer profiles have different effective thicknesses. However, figure 6 compares the numerical Pridmore-Brown modes (figure 6*a*) and the Full Modified Myers approximation (figure 6*b*) for the tanh boundary layer profile with $\delta = 10^{-3}$ and the linear profile with $h = 10^{-3}$, $h = 1.39 \times 10^{-3}$, and $h = 1.5 \times 10^{-3}$; these three linear profiles match the δ_1, $\delta_{\rm mom}$ and $\delta_{\rm ke}$ of the tanh profile respectively. While it is interesting to note the significant motion of the surface modes in region $\mathcal{R}_2$ (the upper-left quadrant of the k-plane), for both the numerical solution and the full modified Myers approximation all three linear profiles support a surface mode in region $\mathcal{R}_1$ (the upper-right quadrant of the k-plane) while the tanh profile does not. This demonstrates that the shape of the boundary layer profile can have an important effect on the presence or absence of this (probably unstable) surface mode.

Finally, we consider the motion of modes as $\mathrm{Im}(Z)$ varies with $\mathrm{Re}(Z)$ fixed (as considered by, for example, Vilenski & Rienstra[20]), since this is the typical situation that occurs with, for example, a Helmholtz Resonator impedance[21] where $\mathrm{Re}(Z)$ is fixed and $\mathrm{Im}(Z)$ varies strongly with frequency and tuning parameters (such as the depth of the resonator cell). Figure 7 shows such a situation with $\mathrm{Re}(Z) = 0.75$, again for the parameters $(\omega, m) = (31, 24)$. The value of $\mathrm{Re}(Z) = 0.75$ was chosen to demonstrate a range of behaviours of surface modes, informed by figure 1; for example, this range of Z passes close to both singularities in figure 1*a*. Of the five surface modes shown in figure 7, the two closest to the origin are accurately predicted by all methods. The surface mode in the $\mathcal{R}_2$ region (the upper-left of the k-plane) is notably less accurately predicted, though is still arguably well-predicted quantitatively. In the $\mathcal{R}_1$ region (the upper-right quadrant of the k-plane), one surface mode is accurately predicted and the other is qualitatively well predicted by both the surface mode dispersion relation (11) and the short wavelength modified Myers dispersion relation, both of which agree very closely with one another. However, both of these methods fail to predict the disappearance of these surface modes behind the critical layer branch cut — a feature demonstrated by the numerical Pridmore-Brown solution and also captured by the full modified Myers boundary condition. This shows that the δI_1 integral is strongly connected with the behaviour of the critical layer branch cut, as predicted in Ref. 13.

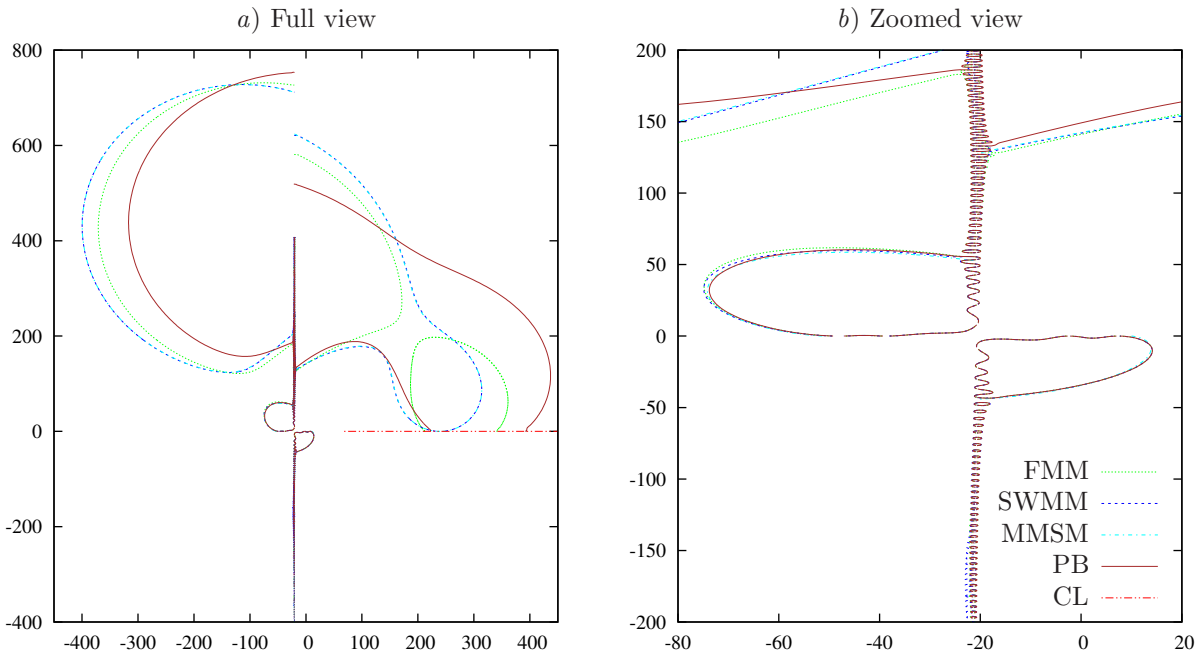

Figure 7. Trajectories of axial wavenumbers (k) in the complex k-plane as $\mathrm{Im}(Z)$ is varies with $\mathrm{Re}(Z) = 0.75$. Parameters are as for figure 5: a tanh boundary layer profile with $\delta = 10^{-3}$ and $M = 0.5$, with $\omega = 31$ and $m = 24$. Solutions are for FMM = Full Modified Myers, SWMM = Short Wavelength Modified Myers, MMSM = Modified Myers Surface Mode, and PB = Pridmore-Brown numerical modes, with CL labelling the critical layer branch cut.

The fact that the full modified Myers solution and the numerical Pridmore-Brown solution show different trends in the upper-right k-plane is explained by the close proximity of the unlabelled singularity in figure 1, which the full modified Myers solution has placed on the wrong side of the line $\mathrm{Re}(Z) = 0.75$.

V. Stability

In this section, we will consider a simplified Briggs–Bers[16,17] stability analysis of the surface modes, similar to that performed in Ref. 13. This stability analysis involves smoothly varying ω, with the imaginary part going from being large and negative to zero and the real part held fixed; here, we assume $\mathrm{Im}(\omega) = -100$ is sufficiently negative. Modes are considered to be left-propagating (upstream propagating) if they originated in the upper-half k-plane, and right-propagating (downstream propagating) if they originated in the lower-half k-plane. This stability analysis presented here is simplified, in that we will not search for absolute instabilities (for further details of a full stability analysis, see, e.g., Ref. 13).

In order to vary ω, the dependence of Z on ω is needed. Here, we choose a Helmholtz resonator impedance model[21] of the form

$$Z(\omega) = \mathcal{R} + \mathrm{i}\omega dL - \mathrm{i}\cot(\omega L), \tag{18}$$

where d is the added mass of the facing sheet nondimensionalized by the mean flow centerline density and the resonator depth, and L is the resonator depth nondimensionalized by the duct radius. Here, we take $d = 4/7$ (as in Refs. 10 and 13) and vary L to give the required impedance at the given frequency.

Figure 8 shows the Briggs–Bers trajectories as $\mathrm{Im}(\omega)$ is varied from -100 to 0 with $\mathrm{Re}(\omega) = 10$ fixed, for the same parameters as figure 3. Four of the five surface modes and all the acoustic modes are seen to be stable, with the only (for this impedance) surface mode in region $\mathcal{R}_1$ (the upper-right quadrant of the k-plane) being a downstream-propagating instability. This is in line with Refs. 6, 10 and 13.

Figure 9 shows the Briggs–Bers stability analysis for the modes in figure 4*a*. This figure shows the lower surface mode in region $\mathcal{R}_1$ (the upper-right quadrant of the k-plane) as being a downstream-propagating convective instability and the other surface mode as being an upstream-propagating stable mode. However, note that by varying the impedance around the singular point in the complex Z-plane (similar to the

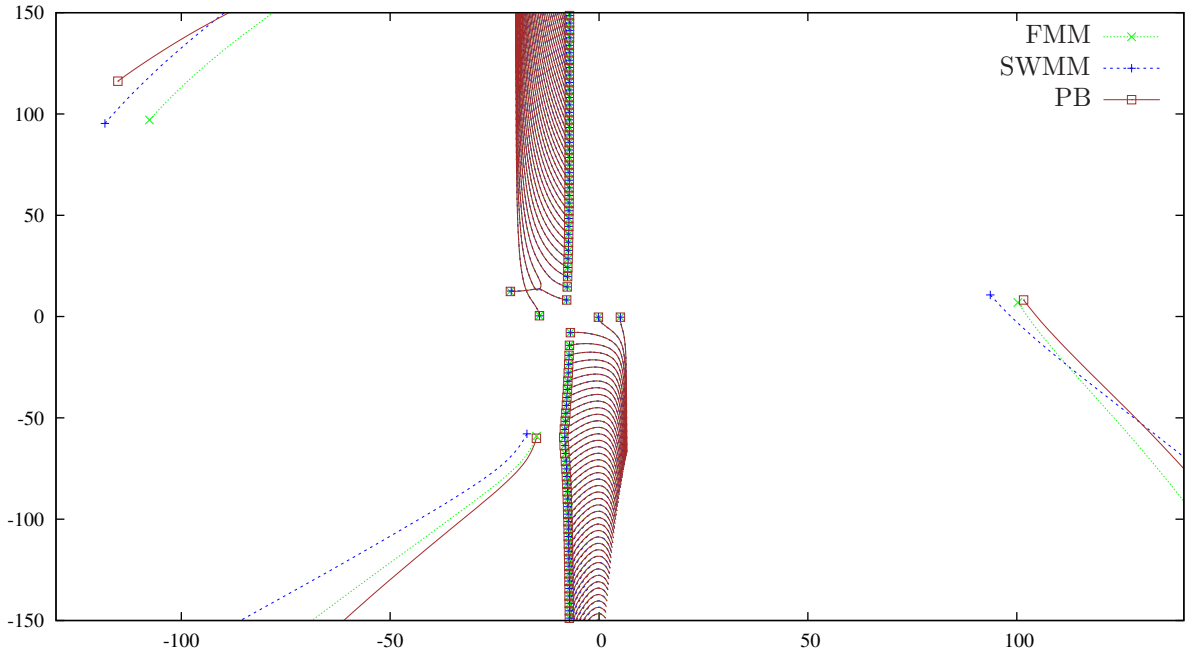

Figure 8. Briggs–Bers trajectories of modes in the complex k-plane for $\mathrm{Im}(\omega) \in [-100, 0]$ with $\mathrm{Re}(\omega) = 10$ for various dispersion relations. Parameters are as for figure 3: $m = 5$, a tanh boundary layer profile (16) with $\delta = 10^{-3}$ and $M = 0.5$, and a Helmholtz resonator impedance (18) with $\mathcal{R} = 1$, $d = 4/7$ and $L = 3.544024 \times 10^{-2}$. Dispersion relations: FMM = Full Modified Myers, SWMM = Short Wavelength Modified Myers, PB = Pridmore-Brown numerical modes.

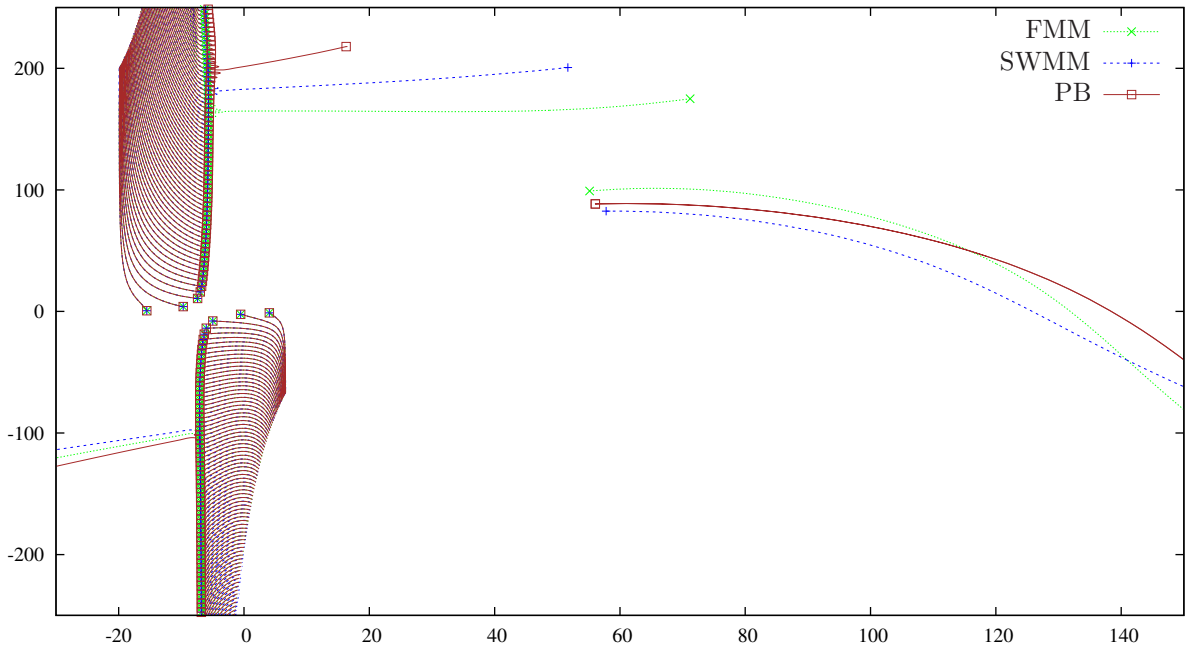

Figure 9. Briggs–Bers trajectories of modes in the complex k-plane for $\mathrm{Im}(\omega) \in [-100, 0]$ with $\mathrm{Re}(\omega) = 10$ for various dispersion relations. Parameters are as for figure 4*a*: $m = 5$, a tanh boundary layer profile (16) with $\delta = 10^{-3}$ and $M = 0.5$, and a Helmholtz resonator impedance (18) with $\mathcal{R} = 1$, $d = 4/7$ and $L = 0.11446$. Dispersion relations: FMM = Full Modified Myers, SWMM = Short Wavelength Modified Myers, PB = Pridmore-Brown numerical modes.

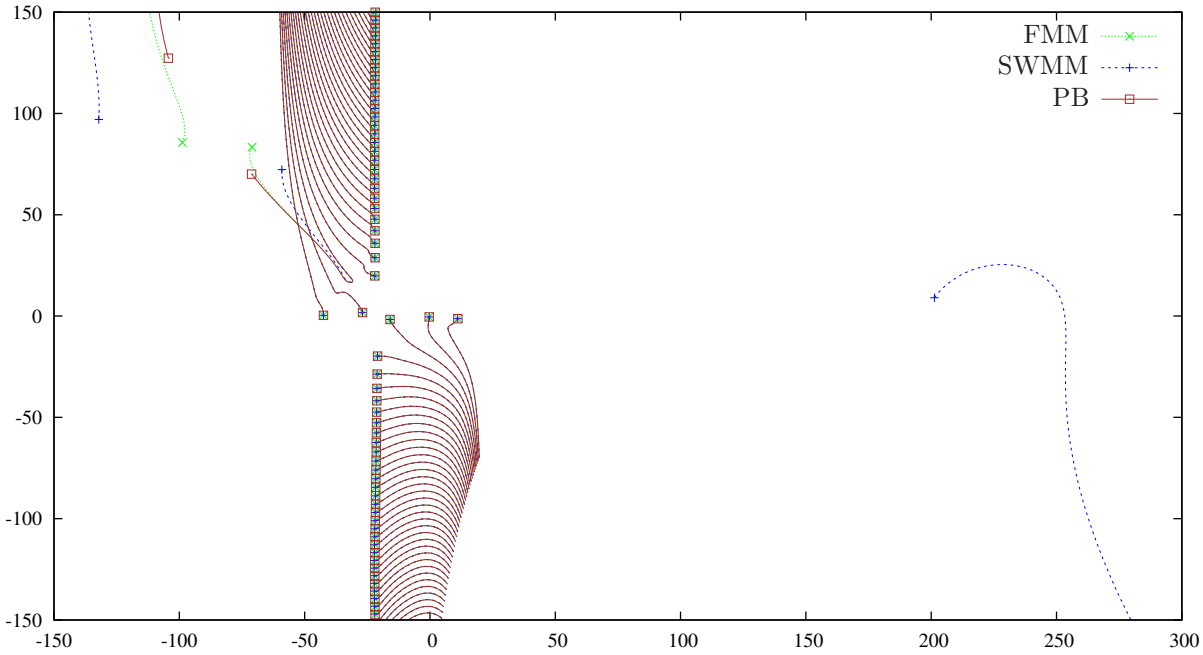

Figure 10. Briggs–Bers trajectories of modes in the complex k-plane for $\mathrm{Im}(\omega) \in [-100, 0]$ with $\mathrm{Re}(\omega) = 31$ for various dispersion relations. Parameters are as for figure 5*a*: $m = 24$, a tanh boundary layer profile (16) with $\delta = 10^{-3}$ and $M = 0.5$, and a Helmholtz resonator impedance (18) with $\mathcal{R} = 1$, $d = 4/7$ and $L = 0.109365$. Dispersion relations: FMM = Full Modified Myers, SWMM = Short Wavelength Modified Myers, PB = Pridmore-Brown numerical modes.

unlabelled singular point in figure 1) these two $\mathcal{R}_1$ surface modes can be made to exchange places, hinting at the existence of an absolute instability in this case for at least some impedances.

Even more confusingly, figure 10 shows the Briggs–Bers stability analysis for the modes in figure 5*a*. In this case, for the full modified Myers and the numerical Pridmore-Brown dispersion relations, the surface mode in region $\mathcal{R}_1$ is hidden behind the branch cut, while for the short wavelength modified Myers dispersion relation this surface mode would be a downstream-propagating convective instability. Note that this surface mode does exist if the boundary layer profile is taken as linear (see figure 6), and in this case a similar analysis shows this surface mode to be a downstream-propagating convective instability.

That one of the surface modes in region $\mathcal{R}_1$ (the upper-right quadrant of the k-plane) seems to always be an instability, and is predicted to always be present for any impedance (although it may in fact be hiding behind the critical layer branch cut) is in line with Refs. 6, 10 and 13, and also with the observations of Ref. 14 for thicker linear boundary layers.

VI. Conclusion

This paper considers the problem of determining the modes, and in particular the surface modes, of a cylindrical lined duct with coaxial flow and a thin sheared boundary layer. The surface mode approximation developed by Rienstra[6] and Brambley & Peake[7] is extended, with the thin boundary layer accounted for using a modified Myers boundary condition in the form proposed by Ref. 13, which is asymptotically correct to first order in the boundary layer thickness for arbitrary boundary layer profiles. The resulting dispersion relation is given in its most readily-useable form in (11), although a rescaled version given in (14) shows the number of free parameters in (11) may be reduced by one. These free parameters are: the lining impedance Z; the centerline Mach number M; the acoustic parameter $\lambda = \omega/\big(m(1-M^2)^{1/2}\big)$; the boundary layer thickness measured on the lengthscale of a far field wavelength $\tilde{h} = 2\omega\delta_{\mathrm{mom}}$; and the boundary layer shape parameters $\Delta_{\mathrm{mass}} = \delta_{\mathrm{mass}}/(2\delta_{\mathrm{mom}})$, $\Delta_{\mathrm{ke}} = \delta_{\mathrm{ke}}/(2\delta_{\mathrm{mom}})$, and $\Delta_1 = -M/\big(2R(1)U'(1)\delta_{\mathrm{mom}}\big)$. The first three parameters, Z, M and λ, are the same as for the uniform flow surface mode approximation.[7] Rather than the four surface modes predicted by the uniform flow surface mode dispersion relation, the sheared flow surface mode

dispersion relation (11) is shown to support up to six surface modes, as described for particular parameters in figures 1 and 2. This helps explain the patterns seen numerically by Vilenski & Rienstra[20] (for example, figure 8*b* of Ref. 20).

For the uniform flow surface mode approximation, as $\mathrm{Im}(Z) \to -\infty$ four surface modes are present, with two surface modes tending to infinity in the k-plane, while as $\mathrm{Im}(Z) \to \infty$ no surface modes are present. The caused Rienstra (section 6 of Ref. 6) to propose a method of finding all modes by tracking modes from their hard-walled values as $\mathrm{Im}(Z)$ is reduced from $+\infty$. With a boundary layer present, we find that there are two surface modes tending to two finite values of k as $|Z| \to \infty$ in any direction (provided $\mathrm{Re}(Z) > 0$), with at least one of these values not corresponding to a hard-walled mode. It would seem, therefore, that this tracking procedure need not to be restricted to reducing $\mathrm{Im}(Z)$ from $+\infty$ but does need to be augmented by finding at least one of the surface modes by independent means.

The fact that the modified Myers boundary condition leads to a maximum of six surface modes, rather than the four predicted for uniform flow is important not only for finding all the modes for a given set of parameters, but also for ascertaining stability. Indeed, the surface mode dispersion relation (11) shows that there are two modes in a region of the k-plane (labelled $\mathcal{R}_1$ in figure 1) that was predicted for uniform flow to contain only one, possibly unstable, surface mode. The stability analysis of section V suggests that one of these surface modes is indeed a downstream-propagating instability while the other is a stable upstream-propagating evanescent wave. These two modes may collide for a particular impedance, labelled as a singularity in figure 1, and will interchange places as the impedance varies around this singularity. This means it is difficult to attach labels to these modes and say one is stable and the other unstable. It is hypothesised here that this behaviour may indicate a possible absolute instability, although this is not investigated further here.

The differential equation governing the pressure in a sheared flow is the Pridmore-Brown equation (17). Approximate solutions to this equation are found in this paper using a number of methods, being (in order of complexity and accuracy): directly numerically integrating the Pridmore-Brown equation (the PB results in figures); solving the modified Myers boundary condition of Brambley,[13] derived asymptotically to include first order effects in the boundary layer thickness (the FMM results in figures); solving a short wavelength approximation to this modified Myers boundary condition (the SWMM results in figures); and assuming the flow to be constant and applying the Myers,[1] or Ingard–Myers,[2] boundary condition (the Myers results in figures). One results of this paper is therefore a comparison of these four methods for a number of different parameters. Unsurprisingly, the more complicated the method the more accurate the results, although the results here confirm the conclusions of Ref. 13 that the Myers boundary condition with uniform flow is a good approximation for the acoustic modes and a rather poor approximation for surface modes.

Section IV gives a range of examples for particular parameters. While all of these examples have $M = U(0) = 0.5$ and $R(r) \equiv 1$, the analysis presented here is valid for general U and R. Two boundary layer profiles were used: the constant-then-linear profile (15) and the tanh profile (16), as used by Vilenski & Rienstra.[20] In general these two boundary layer profiles give similar results. However, as shown in figure 6, it is possible to find parameters for which the linear profile supports an unstable surface wave while the tanh profile does not; moreover, this effect is shown here to be due to the difference in boundary layer profile and not because one boundary layer is effectively thinner than the other. Further investigation is ongoing into the stability implications of this.

For the surface modes, the examples of section IV show very good agreement between the full modified Myers solutions and the direct numerical solutions of the Pridmore-Brown equation, and generally very good agreement in the majority of cases between these and the short wavelength solution and the surface mode solution given by (11); the unmodified Myers solution and its corresponding surface mode approximation show much worse accuracy for the surface modes, and indeed miss two surface modes entirely. While this good accuracy for the modified equations might be seen to be due to the very thin boundary layer used, in fact the small parameter of interest is the scaled boundary layer thickness $\tilde{h}$ given in (12), which for the examples given here is $\tilde{h} \approx 0.04$, which is not enormously small.

One aspect ignored by the current work is the presence of a critical layer and its associated branch cut in the complex k-plane. This branch cut is hinted at in figure 5 and shown explicitly in figure 7, since numerical solutions of the Pridmore-Brown equation and solutions of the full modified Myers dispersion relation are seen to "hide" behind this branch cut for certain values of the impedance Z. Investigation of the critical layer necessitates a different approach, and this is considered for linear boundary layer profiles in Ref. 14.

Acknowledgements

Useful conversations with Prof. S.W. Rienstra are gratefully acknowledged. The author was supported during this work by a Junior Research Fellowship from Gonville & Caius College, Cambridge.

References

[1]Myers, M. K., "On the Acoustic Boundary Condition in the Presence of Flow," *J. Sound Vib.*, Vol. 71, 1980, pp. 429–434.

[2]Ingard, U., "Influence of Fluid Motion Past a Plane Boundary on Sound Reflection, Absorption, and Transmission," *J. Acoust. Soc. Am.*, Vol. 31, 1959, pp. 1035–1036.

[3]Eversman, W. and Beckemeyer, R. J., "Transmission of Sound in Ducts with Thin Shear Layers — Convergence to the Uniform Flow Case," *J. Acoust. Soc. Am.*, Vol. 52, 1972, pp. 216–220.

[4]Tester, B. J., "The Propagation and Attenuation of sound in Lined Ducts containing Uniform or "Plug" Flow," *J. Sound Vib.*, Vol. 28, 1973, pp. 151–203.

[5]Rienstra, S. W., "Hydrodynamic Instabilities and Surface Waves in a Flow over an Impedance Wall," *Proc. IUTAM Symposium 'Aero- and Hydro-Acoustics'*, edited by G. Comte-Bellot and J. E. Ffowcs Williams, Springer, Heidelberg, 1985, pp. 483–490.

[6]Rienstra, S. W., "A Classification of Duct Modes based on Surface Waves," *Wave Motion*, Vol. 37, 2003, pp. 119–135.

[7]Brambley, E. J. and Peake, N., "Classification of Aeroacoustically Relevant Surface Modes in Cylindrical Lined Ducts," *Wave Motion*, Vol. 43, 2006, pp. 301–310.

[8]Brambley, E. J., "Fundamental Problems with the Model of Uniform Flow over Acoustic Linings," *J. Sound Vib.*, Vol. 322, 2009, pp. 1026–1037.

[9]Rienstra, S. W. and Darau, M., "Mean Flow Boundary Layer Effects of Hydrodynamic Instability of Impedance Wall," *Proc. IUTAM Symposium on Computational Aero-Acoustics for Aircraft Noise Prediction, Southampton, 29–31 March*, 2010.

[10]Rienstra, S. W. and Darau, M., "Boundary-Layer Thickness Effects of the Hydrodynamic Instability along an Impednace Wall," *J. Fluid Mech.*, Vol. 671, 2011, pp. 559–573.

[11]Joubert, L., *Asymptotic Approach for the Mathematical and Numerical Analysis of the Acoustic Propagation in a Strong Shear Flow*, Ph.D. thesis, École Polytechnique, 2010, (in French).

[12]Brambley, E. J., "A Well-posed Modified Myers Boundary Condition," AIAA paper 2010-3942, 2010.

[13]Brambley, E. J., "A well-posed boundary condition for acoustic liners in straight ducts with flow," *AIAA J.*, Vol. 49, No. 6, 2011, pp. 1272–1282.

[14]Brambley, E. J., Darau, M., and Rienstra, S. W., "The Critical Layer in Sheared Flow," AIAA paper 2011-2806, 2011.

[15]Brambley, E. J. and Peake, N., "Stability and Acoustic Scattering in a Cylindrical Thin Shell Containing Compressible Mean Flow," *J. Fluid Mech.*, Vol. 602, 2008, pp. 403–426.

[16]Briggs, R. J., *Electron-Stream Interaction with Plasmas*, chap. 2, MIT Press, 1964.

[17]Bers, A., "Space–Time Evolution of Plasma Instabilities — Absolute and Convective," *Basic Plasma Physics*, edited by A. A. Galeev and R. N. Sudan, Vol. 1 of *Handbook of Plasma Physics*, North-Holland, 1983, pp. 451–517.

[18]Rienstra, S. W. and Vilenski, G. G., "Spatial Instability of Boundary Layer Along Impedance Wall," AIAA paper 2008-2932, 2008.

[19]Pridmore-Brown, D. C., "Sound Propagation in a Fluid Flowing Through an Attenuating Duct," *J. Fluid Mech.*, Vol. 4, 1958, pp. 393–406.

[20]Vilenski, G. G. and Rienstra, S. W., "Numerical Study of Acoustic Modes in Ducted Shear Flow," *J. Sound Vib.*, Vol. 307, 2007, pp. 610–626.

[21]Rienstra, S. W., "Impedance Models in Time Domain, including the Extended Helmholtz Resonator Model," AIAA paper 2006-2686, 2006.